Projection Center Calibration for a Co-located Projector Camera System

Toshiyuki Amano
Department of Computer and Communication Science
Faculty of Systems Engineering, Wakayama University
Sakaedani 930, Wakayama, 640–8510, Japan
amano@sys.wakayama-u.ac.jp

Abstract

A co-located projector camera system where the projector and camera are positioned in the same optical position by a plate beam splitter enables various spatial augmented reality applications for dynamic three dimensional scenes. The extremely precise alignment of the projection centers of the camera and projector is necessary for these applications. However, the conventional calibration procedure for a camera and projector cannot achieve high accuracy because an iterative verification process for the alignment is not included. This paper proposes a novel interactive alignment approach that displays a capture of the projected grid pattern on the calibration screen. Additionally, a misalignment display technique that employs projector camera feedback is proposed for fine adjustment.

1. Introduction

A projector camera system that consists of a camera and projector enables not only the irradiance compensation of the projection onto an arbitrary surface, but also the manipulation of its appearance, human computer interaction, projection mapping, etc. Generally, a geometrical calibration is applied to obtain a pixel mapping between the projection and captured image before projector camera feedback. Since it inhibits successive projections, the offline calibration method that uses a calibration pattern projection to find corresponding pixels cannot be applied dynamically.

One solution for this problem is adaptive geometrical calibration for a non co-located projector camera system. Johnson et al. [7] and Audet et al. [4] proposed dynamic geometrical calibration methods. These methods are promising solutions for projection on a moving surface. However, they require a shape model of the target.

Another solution is the employment of a co-linear projector camera system that divides the projection and the imaging with a plate beam splitter (PBS). The co-linear optics, more accurately the optics that place both projection

centers in same position, do not require an adaptive geometrical calibration and allow us not only dynamic adaptation of irradiance compensation [5] but also many applications [11, 6, 10]. The success of these applications depending on the alignment accuracy of the projector and camera. In particular, the projector camera feedback application such as [5, 1] require alignment to sub-pixel accuracy. The camera and projector calibration method [3, 9, 8] is usable for the alignment, but it cannot get success because it contains errors in projection centers estimation. Zhang et al. [11] proposed methods for enhanced image display based on projection defocus-analysis that employed a coaxial projector camera system. In their research, an image projection onto a white screen with a fence is used and finding the camera position where a cast shadow is removed has been proposed for the camera alignment. We nevertheless need to discuss on it to achieve sub-pixel accuracy with the general approach.

This paper proposes an interactive position alignment for projection centers. Its novel contribution is misalignment visualization using the projector camera feedback. Since a small misalignment generates artifact pattern with the projector camera feedback, we can easily achieve highly accurate alignments.

2. Projector Camera System Geometry

Projection center alignment is the task of adjusting the relative position between projector and camera. For this problem, we place the world coordinates along the projection model of the projector as shown in fig. 1. The homography between the captured image coordinates coordinate $\tilde{\mathbf{m}}_c = [x_c, y_c, 1]^T$ and world coordinates on the $Z = Z_1$ plane $\tilde{\mathbf{g}} = [X, Y, 1]^T$ is

$$\tilde{\mathbf{m}}_c \propto \mathbf{A}_c \left[\mathbf{r}_{c1}, \mathbf{r}_{c2}, \mathbf{t}_c + Z_1 \mathbf{r}_{c3} \right] \begin{bmatrix} X \\ Y \\ Z_1 \\ 1 \end{bmatrix} \quad (1)$$
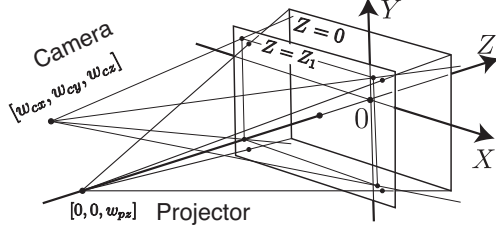$$\equiv \mathbf{A}_c \mathbf{\Phi}(Z_1) \tilde{\mathbf{g}}$$

Figure 1. Position of camera and projector projection centers. The Z axis of the world coordinates is defined to correspond with the optical axis of the projector and the X and Y axes are defined as parallel to x_p and y_p, respectively.
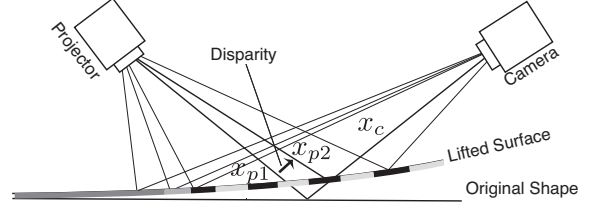

Figure 2. The generating mechanism of artifact pattern. A disparity between captured image and projection images that caused for the misalignment from the initial calibration setting makes stripe artifact pattern.

using a Zhang's camera model [12], where $\mathbf{t}_c$ is a translation vector that has a direction opposite that of the position vector $\mathbf{w}_c = [w_{cx}, w_{cy}, w_{cz}]$ such that $\mathbf{t}_c = -\mathbf{w}_c$. Columns $\mathbf{r}_{c1}, \mathbf{r}_{c2}, \mathbf{r}_{c3}$ are the columns of rotation matrix $\mathbf{R}_c$, and the matrix $\mathbf{A}_c$ contains the intrinsic camera parameters. In a similar way, the homography between a projection image $\tilde{\mathbf{m}}_p$ and $\tilde{\mathbf{g}}$ is

$$
\tilde{\mathbf{m}}_p \propto \mathbf{A}_p \begin{bmatrix} 1 & 0 & 0 \\ 0 & 1 & 0 \\ 0 & 0 & t_{pz} + Z_1 \end{bmatrix} \begin{bmatrix} X \\ Y \\ 1 \end{bmatrix} \tag{2}
$$
$$
\equiv \mathbf{A}_p \boldsymbol{\Psi}(Z_1) \tilde{\mathbf{g}},
$$

where $t_{pz} = -w_{pz}$, and $\mathbf{A}_p$ contains the intrinsic parameters. From the combination of these homographies, we get

$$
\mathbf{H}'_{p2c} = \mathbf{A}_c \left[\mathbf{r}_{c1}, \mathbf{r}_{c2}, \frac{1}{t_{pz} + Z_1}(\mathbf{t}_c + Z_1 \mathbf{r}_{c3}) \right] \mathbf{A}_p^{-1}. \tag{3}
$$

In particular, this homography can be described as

$$
\mathbf{H}_{p2c} = \mathbf{A}_c \left[\mathbf{r}_{c1}, \mathbf{r}_{c2}, \frac{1}{t_{pz}} \mathbf{t}_c \right] \mathbf{A}_p^{-1}, \tag{4}
$$

for the projection plane $Z = 0$.

When both projection centers are placed in same position, $\mathbf{H}_{p2c}$ and $\mathbf{H}'_{p2c}$ are identical.

3. Misalignment Visualization

We attempt a successive photometric compensation by the projector camera feedback that was proposed by Fujii et al. [5]. We then confirm alignment from the observation of occurring visual artifacts when the both projection centers are incoincident. The photometric compensation combines a model based approach of the projector camera response with dynamic feedback between capture and projection. It allows us photometric compensation in a dynamic environment. That is an illumination from the projector is adjusted by the negative feedback according to the captured brightness, and a geometrical pixel mapping between the capture

and projection is required in order to apply optical feedback. However, when the mapping includes misalignment it will fail immediately and the system generates stripe shape artifact pattern.

Consider a camera pixel x_c captures x_{p1} on the original shape and the captured projection is slightly changed to x_{p2} by the disparity caused by displacement of the screen as shown in figure 2. The artifact is generated by an incorrect pixel mapping during the projector camera feedback. When a camera pixel at x_c captures the projection illumination from x_{p2} and it is slightly darker from desired brightness, the illumination from x_{p1} will be increased step by step and it will reach maximum illumination. Since the illumination on x_{p1} is enough bright, the opposite mechanism occurs on next neighboring pixel pairs. As a result, an incorrect pixel mapping creates a stripe artifact pattern, where its pattern direction indicates the direction of disparity. In this paper, the color saturation reduction [2] is applied as a projector camera feedback for its high visibility of artifact.

4. Interactive Projector Camera Alignment

Figure 3 illustrates the system optics. The system consists of a high dimensional (HD) resolution 3LCD projector, IEEE1394 digital camera with 1600×1000 pixels, a PBS, and a stray light absorber. The camera and the projector can be optically aligned to the same position using the PBS. Elements w_{cx} and w_{cz} are adjusted by positioning of the camera unit and w_{cy} is adjusted by the back and forth movement within the camera unit. In order to observe two projections on $Z = 0$ and $Z = Z_1$ simultaneously, we place the slit screen shown in figure 4(a) that has many line-shaped openings at $Z = Z_1$ in front of the calibration plane $Z = 0$. The projector and slit screen are placed at $w_{pz} = -1200mm$ and $Z_1 = -20mm$ in front of the planar screen $Z = 0$. We then move the camera unit continuous grid lines appear on the captured image.

Figure 5 shows the calibration progress. In the initial position, we can see continuous horizontal lines in the captured image, but the vertical lines are discontinuous. This suggests the camera is misaligned in the direction of the
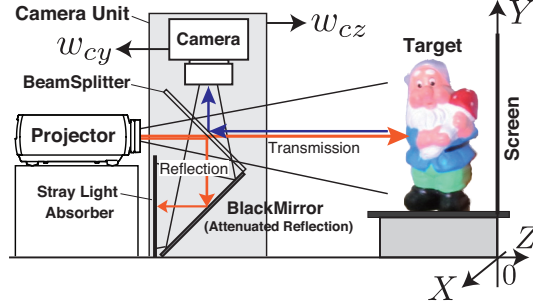
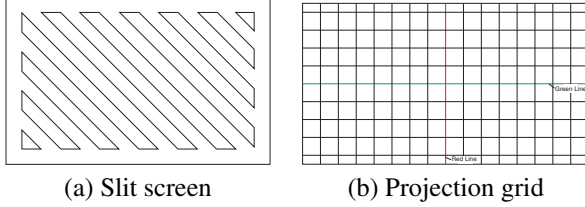Figure 3. Optical layout of the projector camera system.

(a) Slit screen   (b) Projection grid

Figure 4. Calibration screen and grid pattern. (a) The slit screen is placed at Z=Z1 in front of the planar screen Z=0. (b) The grid pattern is used to verify the alignment of the projection centers.

horizontal axis, and we get stripe-shaped artifact as a result of projector camera feedback, as shown on the right side of figure 5(a). Therefore, we move the camera approximately $-30mm$ in the direction of the X axis at the step 1. It is easy to determine the direction needed to align the camera projection center from the homography in the section 2 using the approximation procedure without the camera rotation term. Note that, the condition $\mathbf{R}_c \approx \mathbf{I}$ is needed to determine rough manipulation direction, but a perfect fronto-parallel is not required for initial condition. The detailed procedure is described below.

Case 1: $w_{cz} = w_{pz}$

In this case, we can alter the continuity of the vertical projection lines by the movement of the camera unit in the X direction. To alter the continuity of the horizontal projection lines, we can adjust the Y position by the moving the camera within the camera unit in the w_{cy} direction.

Case 2: $w_{cx} = w_{cy} = 0$

In this case, the scales of the projected grid patterns on $Z = 0$ and $Z = Z_1$ are different. Because different projection distances from different size grids in the captured image, we move the camera unit forwards or backwards in the Z direction to get the same scale grid patterns in the captured image.

Case 3: All of w_{cx}, w_{cy}, w_{cz} **are misaligned.**

Because the angle of view of common projectors (or cameras) is not very wide (approximately 30 degrees),

(a) Initial position

(b) Step 1 (t_{cx} direction $\approx -30mm$)

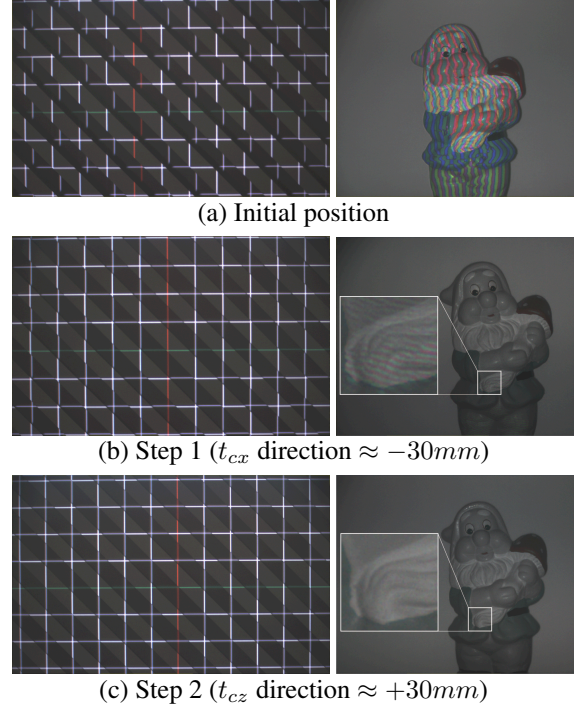(c) Step 2 (t_{cz} direction $\approx +30mm$)

Figure 5. Calibration progress. The left side images shows captured image when we project grid pattern on the $Z = 0$ plane through the slit screen. The right side image shows appearance manipulation results with projector camera feedback that aimed to reduce color saturation in optically.

misalignment of w_{cx} and w_{cy} significantly affects the continuity of the grid lines more than the misalignment of w_{cz}. Therefore, we first attempt to adjust w_{cx} and w_{cy} by the procedure described in case 1 before attempting the procedure described in case 2.

We can see nearly continuous grid lines in the result shown in figure 5(b), however, the grid intervals on the $Z = 0$ and $Z = Z_1$ planes are slightly different. Because the projector camera feedback is applied by the pixel-parallel processing, a small misalignment creates an incorrect pixel mapping and produces an artifact in regions not on the $Z = 0$ plane. This is because the pixel map between a projector and camera is calibrated on the $Z = 0$ plane by gray code projection.

In the step 2, we carefully move the camera position in the direction of the Z axis to form the same grid pitch on both screens. Finally, we obtain a perfectly consecutive grid pattern image and appearance as shown in figure 5(c).

5. Fine adjustment by the optical feedback

The interactive calibration is a simple operation that makes it easily to determine the alignment of the camera.
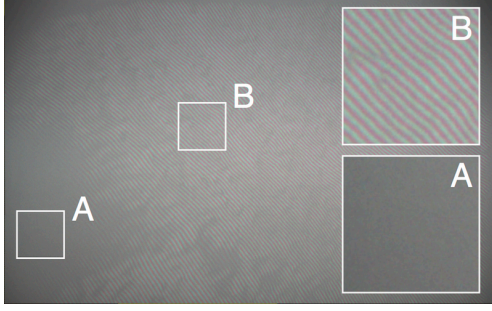
Figure 6. Artifact on the $Z = Z_1$ plane. Since the pixel map for the projector camera feedback was obtained by a gray code projection on $Z = 0$, the artifact arise on $Z = Z_1$ when the projection centers are misaligned.
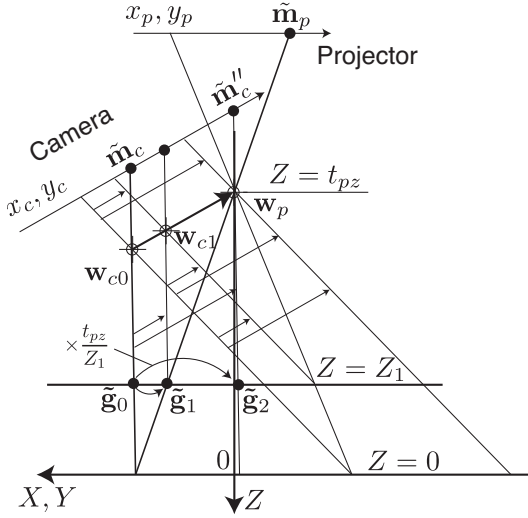

Figure 7. Homography on the $\mathbf{w}_c = \mathbf{w}_p$. When we position the camera to remove artifact patterns caused by the projector camera feedback on $Z = Z_1$, the projection center of the camera moves to $\mathbf{w}_{c1}$ from $\mathbf{w}_{c0}$ in the direction of $\mathbf{w}_p$.

However, because its accuracy depends on human observation of line continuity, it is hard to achieve sub-pixel accuracy of the camera alignment. Figure 6 shows the results of projector camera feedback on the $Z = Z_1$. We can confirm a good control result in region A, but can see an artifact pattern caused by misalignment in region B. This is because the alignment was verified by the projector camera feedback on the target object that was placed between $Z = 0$ and $Z = Z_1$ in the previous result, but the mapping error can increase on $Z = Z_1$ because of its geometrical relation. Next, we attempt a fine adjustment that uses the artifact pattern caused by this misalignment to solve the problem caused by the limits of human ability to observe line continuity.

5.1. Aligned Homography Estimation

Figure 7 illustrates the projection model of a projector camera system with the calibration planes $Z = 0$ and $Z = Z_1$. Consider the situation when the calibration plane $Z = 0$ moves to $Z = Z_1$. As an initial condition, we apply H_{p2c} to the projector camera feedback on the $Z = Z_1$. Since H_{p2c} is a homography on the $Z = 0$, we see the artifact pattern on the $Z = Z_1$, but we can remove this artifact by parallel camera displacement.

When the correct displacement removes the artifact pattern, the camera projection center extended to $\mathbf{w}_{c1}$, the point on the line that connects the $\mathbf{w}_{c0}$ and $\mathbf{w}_p$. From the geometrical relation, the t_{pz}/Z_1 times translation of this moves the camera's projection center to $\mathbf{w}_p$.

The homography on the $Z = 0$ is written as

$$\tilde{\mathbf{m}}_c \mathbf{H}_{p2c} \propto \tilde{\mathbf{m}}_p, \tag{5}$$

and the projection of $\tilde{\mathbf{g}}_0$ by the camera can be expressed by

$$\tilde{\mathbf{g}}_0 \propto \boldsymbol{\Phi}(Z_1)^{-1} \mathbf{A}_c^{-1} \tilde{\mathbf{m}}_c. \tag{6}$$

In the same manner, we get

$$\tilde{\mathbf{g}}_1 \propto \boldsymbol{\Psi}(Z_1)^{-1} \mathbf{A}_p^{-1} \tilde{\mathbf{m}}_p. \tag{7}$$

Further, let $\tilde{\mathbf{g}}_2$ be a point that is the target projection point of $\tilde{\mathbf{m}}_c$ caused by the camera translation. Because $\tilde{\mathbf{g}}_2$ is given by the t_{pz}/Z_1 translations of $\tilde{\mathbf{g}}_1 - \tilde{\mathbf{g}}_0$, it is given by

$$\tilde{\mathbf{g}}_2 = \mathbf{K}(\zeta_1 \tilde{\mathbf{g}}_1 - \zeta_0 \tilde{\mathbf{g}}_0) + \zeta_0 \tilde{\mathbf{g}}_0, \tag{8}$$

where

$$\mathbf{K} \equiv \begin{bmatrix} \frac{t_{pz}}{Z_1} & 0 & 0 \\ 0 & \frac{t_{pz}}{Z_1} & 0 \\ 0 & 0 & 1 \end{bmatrix}, \tag{9}$$

and where ζ_1 and ζ_0 are coefficients to normalize the third element of $\tilde{\mathbf{g}}_1$ and $\tilde{\mathbf{g}}_0$ to 1. From the above equations, the projection of $\tilde{\mathbf{g}}_2$ onto the captured image can be written as

$$\tilde{\mathbf{m}}_c'' \propto \mathbf{A}_c \boldsymbol{\Phi}(Z_1) \tilde{\mathbf{g}}_2$$
$$= \left\{ \mathbf{K}(\zeta_1 \mathbf{H}_{p2c}' - \zeta_0 \mathbf{H}_{p2c}) + \zeta_0 \mathbf{H}_{p2c} \right\} \tilde{\mathbf{m}}_p. \tag{10}$$

Because the direction of camera displacement is counter to the coordinate transformation direction, we get the homography
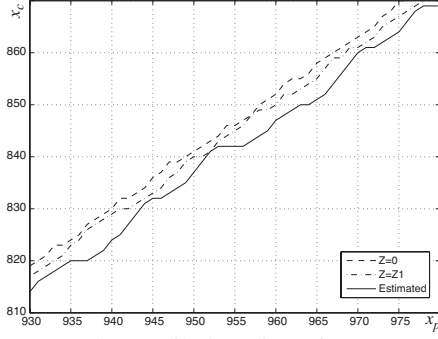
$$\hat{H}_{p2c} = \mathbf{K}(\zeta_1 \mathbf{H}_{p2c}' - \zeta_0 \mathbf{H}_{p2c}) + \zeta_0 \mathbf{H}_{p2c} \tag{11}$$

that aligns the camera's projection center onto $\mathbf{w}_p$.

However, we cannot express $\hat{H}_{p2c}$ as a unique matrix. This is because ζ_0 and ζ_1 depend on each $\tilde{\mathbf{m}}_p$. However, we generally use a pixel map that is expressed by a lookup table instead of a homography matrix. Hence, let $(x_c, y_c) = \mathbf{f}_{p2c}(x_p, y_p)$ and $(x_c, y_c) = \mathbf{f}_{p2c}'(x_p, y_p)$ be a pixel map on

(a) After the interactive calibration.

(b) Detailed section of (a).

Figure 8. Disparity between pixel pixel maps obtained at $Z = 0$ and $Z = Z_1$. (a) Pixel maps obtained at $Z = 0$ and $Z = Z_1$ are close to the target "Estimated". (b) However, we can see that there are approximately two pixels of disparity between these pixel maps and both diverge from the target pixel map.

$Z = 0$ and $Z = Z_1$, respectively. We then obtain a pixel map that moves the camera's projection center to $\mathbf{w}_p$ as

$$\hat{\mathbf{f}}_{p2c} = -\frac{t_{pz}}{Z_1}(\mathbf{f}'_{p2c} - \mathbf{f}_{p2c}) + \mathbf{f}_{p2c}. \tag{12}$$

For this pixel map update, we first rough measure the t_{pz}. Because $\mathbf{f}'_{p2c}$ and $\mathbf{f}_{p2c}$ are close and it is not sensitive to t_{pz}. Furthermore, when a measurable residual error remained we can repeat fine adjustment step to reduce residual error. Then, it does not require precise positioning of calibration plane $Z = Z_1$ if a proper update gain for the update scheme is given.

5.2. Fine Adjustment Results

For fine adjustment, we first obtain two pixel maps of $\mathbf{f}_{p2c}$ and $\mathbf{f}'_{p2c}$ using the conventional gray code projection to obtain $\hat{\mathbf{f}}_{p2c}$. Figure 8 shows a pixel map between x_p and x_c on $y_p = 500$. The lines labeled "Z=0" and "Z=Z1" show the pixel maps obtained on each calibration plane, where "Estimated" is the pixel map that calculated by eq.(12). Because the projection center is roughly adjusted by the interactive projector camera alignment procedure, both pixel
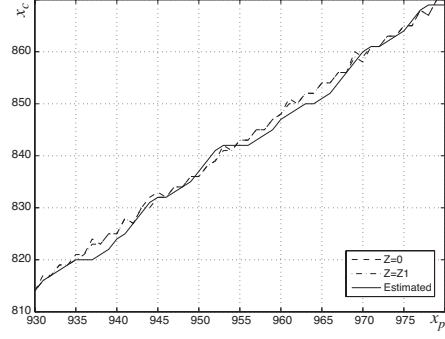

Figure 9. Disparity after the fine adjustment between pixel maps on $Z = 0$ and $Z = Z_1$. These pixel maps overlapped by $\hat{\mathbf{f}}_{p2c}$.
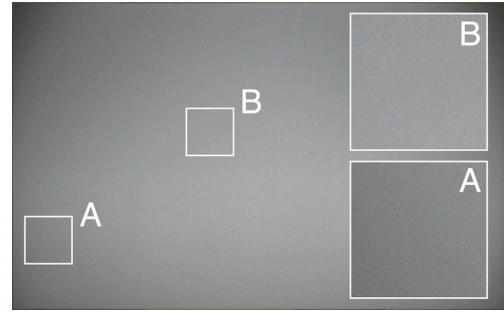

Figure 10. Results on $Z = Z_1$ after the fine adjustment. The artifact pattern caused by misalignment has been removed.

maps are close to each other. However, there is a misalignment of two pixels on average (see table 1) between both pixel maps, creating an artifact pattern on the $Z = Z_1$ plane caused by the projector camera feedback.

Next, we apply $\hat{\mathbf{f}}_{p2c}$ to the projector camera system, moving the camera back and forth and around slightly to determine the position such that the artifact pattern is eliminated. Because the projection center has been roughly adjusted by the previous alignment, the position to remove the artifact pattern is close to the initial position. Therefore, this procedure does not require a large number of trials. Figure 9 shows the pixel map obtained after fine adjustment. Clearly, we can see that both pixel maps overlap each other by $\hat{\mathbf{f}}_{p2c}$, suggesting that the projection center of the camera is perfectly matched to $\mathbf{w}_p$.

Figure 10 shows the result of the projector camera feedback on the $Z = Z_1$ plane with the pixel map obtained at $Z = 0$. Thanks to this fine adjustment, the artifact seen in figure 6 has disappeared, and we can confirm that both projection centers are perfectly aligned from this result.

5.3. Quantitative Evaluation of the Calibration

Table 1 shows the mean average errors (MAEs) and standard deviations between pixel maps obtained at $Z = 0$ and

Table 1. Alignment error of projection centers.

	MAE x_c	MAE y_c	$\sigma-x_c$	$\sigma-y_c$
Initial	34.3	1.28	0.371	0.844
Step 1	2.93	1.84	0.113	0.496
Step 2	2.00	0.710	0.117	0.638
Fine Adj.	0.614	0.548	0.413	0.275

$Z = Z_1$ at each calibration step. The unit of these values is pixels. From this table, it is clear that the MAEs are reduced at each step and calibration procedure is effectively applied. In the final result, we achieved a sub-pixel accuracy mapping in the region $-20 \leq Z \leq 0$ mm in world coordinates. In contrast, an improvement with each calibration step is not seen with respect to the standard deviation σ. This is because σ arises from the roughness of the pixel maps, and it does not depend on the misalignment of the camera. Because the pixel maps are described by the integer-formatted lookup table for its implementation, the $0.113 \leq \sigma \leq 0.844$ is a reasonable rounding error in practice.

The experiment by a non-author (male, 22 years of age who has fundamental knowledge of optics) was performed in two cases. One is a 2-DOF alignment that the user moves the camera unit on the table surface and adjusts w_{cx} and w_{cz}, another is 3-DOF alignment that added w_{cy} adjustment to 2-DOF. The initial displacement was set around 30 mm in each direction. The calibration in case of 2-DOF and 3-DOF took 46 and 57 sec with the gird-pattern projection. In contrast, these calibration durations were reduced to 28 and 26 sec with knowledge shown in section 3 but there was no difference in accuracy (between 0.75 and 1.93 pixel in MAE). The fine adjustment process is time consuming and it required a few minutes to adjust in each trial. However the artifact pattern has been removed and achieved sub-pixel accuracy.

6. Conclusion

A projector camera system that places both projection centers at the same position allows an invariant pixel mapping for projection distance. Therefore, this projector camera system could easily be applied to dynamical spatial AR applications. The key to the success of these applications is the alignment accuracy of the projector and camera. This paper proposed an interactive alignment procedure that used a live grid pattern captured through a slit screen. Using the proposed method, a user can easily determine the position for projection-center alignment. Addition to this, a fine adjustment method based on the optical feedback was proposed. This fine-adjustment shows only misalignment using an artifact pattern, however, when we apply it as a final step of an interactive adjustment, it does not require many trials. As a result, we achieved an alignment with

sub-pixel accuracy after the final adjustment. We believe this calibration technique could be applied not only to augmented reality but also to optical devices for computational photography.

Acknowledgment

References

[1] T. Amano. Real world dynamic appearance enhancement with procam feedback. In *Proc. of the 2nd IEEE International Workshop on Computational Cameras and Displays*, pages 918–923, 2013. 1

[2] T. Amano and H. Kato. Appearance control using projection with model predictive control. In *Proc. of ICPR*, pages 2832–2835. IEEE Computer Society, 2010. 2

[3] M. Ashdown and Y. Sato. Steerable Projector Calibration. *2005 IEEE Computer Society Conference on Computer Vision and Pattern Recognition - Workshops*, 3:98–98. 1

[4] S. Audet, M. Okutomi, and M. Tanaka. Direct image alignment of projector-camera systems with planar surfaces. *2010 IEEE Computer Society Conference on Computer Vision and Pattern Recognition*, pages 303–310, June 2010. 1

[5] K. Fujii, M. Grossberg, and S. Nayar. A projector-camera system with real-time photometric adaptation for dynamic environments. *2005 IEEE Computer Society Conference on Computer Vision and Pattern Recognition (CVPR'05)*, pages 814–821 vol. 1, 2005. 1, 2

[6] D. Iwai and K. Sato. Optical superimposition of infrared thermography through video projection. *Infrared Physics & Technology*, 2010. 1

[7] T. Johnson and H. Fuchs. Real-time projector tracking on complex geometry using ordinary imagery. In *Computer Vision and Pattern Recognition, 2007. CVPR '07. IEEE Conference on*, pages 1–8, June 2007. 1

[8] M. Kimura, M. Mochimaru, and T. Kanade. Projector Calibration using Arbitrary Planes and Calibrated Camera. *2007 IEEE Conference on Computer Vision and Pattern Recognition*, (4):1–2, June 2007. 1

[9] I. Mitsugami, N. Ukita, and M. Kidode. Displaying a Moving Image By Multiple Steerable Projectors. *2007 IEEE Conference on Computer Vision and Pattern Recognition*, pages 1–8, June 2007. 1

[10] K. Okumura, H. Oku, and M. Ishikawa. Active Projection AR using High-speed Optical Axis Control and Appearance Estimation Algorithm. In *Proc. of 2013 IEEE International Conference on Multimedia and Expo (ICME 2013)*, 2013. 1

[11] L. Zhang and S. Nayar. Projection defocus analysis for scene capture and image display. *ACM Trans. Graph.*, 25(3):907–915, July 2006. 1

[12] Z. Zhang. A flexible new technique for camera calibration. *Pattern Analysis and Machine Intelligence, IEEE Transactions on*, 22(11):1330–1334, Nov 2000. 2